Available online at www.sciencedirect.com

ScienceDirect

Procedia CIRP 110 (2022) 2–7

www.elsevier.com/locate/procedia

V CIRP Conference on Biomanufacturing

The Effect Of Machining Cooling Strategies On The Corrosion Fatigue Performances Of the AZ31 Magnesium Alloy

R. Bertolini*[a], HC Jansen[b], A. Ghiotti[a], S. Bruschi[a]

[a]*Dept. Of Industrial Engineering, University of Padova, Via Venezia 1, 35131, Padova, Italy*

[b]*RWTH Aachen University, Templergraben 55, 52056, Aachen, Germany*

* Corresponding author. Tel.: 049 8276818. *E-mail address:* rachele.bertolini@unipd.it

Abstract

Magnesium alloys are very attractive biomaterials thanks to their biocompatibility, nontoxicity, and biodegradability. However, they have not been used extensively until nowadays because of their susceptibility to corrosion especially when in synergy to mechanical loads. In this framework, the present work deals with the analysis of the influence that different machining strategies may have on the corrosion fatigue performances of the AZ31 magnesium alloy. To this aim, cryogenic and dry machining operations were carried out, and the machined samples were then subjected to corrosion fatigue tests in a physiological environment at different imposed stresses, namely 100 MPa, 110 MPa and 120 MPa. The obtained results show that the samples processed with the liquid nitrogen adduction had a higher fatigue life than the corresponding dry samples, regardless of the imposed level of stress. After corrosion fatigue testing, both the types of samples showed similar failure characteristics. However, the microstructures of the cryogenic machined samples were characterized by a lower amount of deformation twins thanks to the grain refinement induced by cryogenic cooling close to the machined surface. Both the grain refinement and the reduced amount of deformation twins were used to explain the enhance corrosion fatigue characteristics of the cryogenic machined samples. These results indicate that cryogenic machining can represent a promising approach to enhance the poor corrosion fatigue behavior of the AZ31 magnesium alloy.

Keywords: AZ31 magnesium alloy; cryogenic machining; corrosion behavior; corrosion fatigue

1. Introduction

Magnesium alloys are emerging as potential candidates for degradable temporary implants because of their mechanical properties that are closer to those of the natural bone compared to other metals, their good biocompatibility, nontoxicity, and biodegradability. However, once placed in the human body, they tend to corrode too quickly, loosening their structural stability before the end of the period of complete healing. Therefore, the rapid degradation in physiological environment limits the clinical applications of these alloys to a great extent. In recent years, the research studies dealing with clinical applications of the magnesium alloys have been mainly concerned on reducing their corrosion degradation rate [1]. However, not only wthe aggressive physiological environment, but also the mechanical loads the temporary implants may be subjected may contribute to a further shortening of their in-service lifetime. These mechanical loads may be either tensile, inducing Stress Corrosion Cracking (SCC), or cyclic, inducing Corrosion Fatigue (CF).

Although several literature studies are available about SCC [2,3], only a few can be found about CF.

Gu et al. [4] systematically investigated the CF behavior of the die-cast AZ91D and extruded WE43 alloys in a Simulated Body Fluid (SBF) environment. They found that the latter alloy was characterized by greater fatigue strength thanks to its finer microstructure. Indeed, the reduced grain size after extrusion resulted in crack initiation inhibition, due to the dislocation

10.1016/j.procir.2022.06.003

motion impair and increase in the number of barriers to early crack propagation. Autunes et al. [5] underlined the positive influence of residual compressive stresses on the corrosion fatigue of metal alloys as fatigue cracks tend to originate from zones affected by residual tensile stresses in correspondence of the free surface of the metal. In [6], the CF behavior of coarse grained and Surface Mechanical Attrition Treated (SMAT) AZ31B magnesium alloy was investigated, showing improved fatigue performance of the SMAT specimens over coarse grained specimens thanks to the formation of a nanocrystalline surface layer, the development of a work-hardened area, and the introduction of residual compressive stresses on the surface.

All the above-mentioned studies indicate that the surface status plays the primary role in determining the in-service properties of magnesium alloys. To this regard, Severe Plastic Deformation (SPD) processes [7], among which machining and burnishing, can be exploited to suitably modify the surface characteristics of magnesium alloys. Especially machining represents a promising strategy since it is usually included within the manufacturing chain of whatever components, implants included. In previous works of the Authors [8, 9], the effects of dry and cryogenic machining on the surface integrity and corrosion resistance of AZ31 magnesium alloy were investigated. It was found a 24% thickness increase of the SPD layer, which consists in a finer grains zone compared to the bulk material, in case of cryogenic machined samples as well as five times thicker nanoscale layer over dry machined samples. Additionally, a residual compressive stress state with a maximum of 143 MPa was reported in case of cryogenic machining, while a residual tensile stress state with a maximum of 270 MPa was obtained when dry machining. Thanks to that, it was proved that cryogenic cooling could lead to a reduction of one order of magnitude in the corrosion current density as well as corrosion potential ennoblement when the samples were tested in SBF at 37°C. In a follow-up study [10], the SCC behavior of dry and cryogenic machined samples was evaluated in SBF. The SSC indexes of dry machined samples were nearly 23% and 11% higher than the ones calculated for cryogenic machined ones indicating a lower SSC strength.

From the literature review it emerges that there is a lack of studies dealing with CF behavior of magnesium alloys as well as the feasibility of using cryogenic machining for enhancing the CF performances of magnesium alloys was never investigated. To this aim, AZ31 magnesium alloy samples were dry and cryogenic machined, and, afterwards, subjected to CF tests at varying imposed stress in a physiological environment. After testing, the fracture surfaces microstructural features close to the machined surface were analyzed to be correlated with the CF behaviour.

Nomenclature

SCC	stress corrosion cracking
CF	corrosion fatigue
SBF	simulated body fluid
N_f	number of cycles to failure
σ_a	nominal applied stress amplitude

2. Experimental

2.1. Material

The material under investigation was the commercially available AZ31B magnesium alloy, supplied in form of a bar with 16 mm diameter and 1000 mm length.

The mechanical properties of the as-received material were evaluated using a MTS™-322 hydraulic dynamometer with maximum load of 50 kN. Uni-axial tensile tests were carried out at a strain rate of 0.1 s^{-1} at room temperature. The mechanical characteristics derived from the engineering stress-strain curve of Fig. 1 are summarized in Table 1.

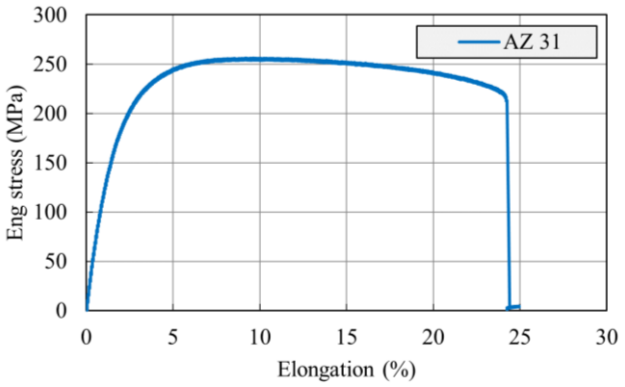

Fig. 1. Engineering stress-strain curve of the AZ31B magnesium alloy at room temperature.

Table 1. Mechanical characteristics derived from Fig. 1.

Yield stress, $\sigma_{p0.2}$ (MPa)	Ultimate tensile stress, UTS (MPa)	Elongation at fracture (%)
144 ± 2	255 ± 3	24 ± 1

2.2. Machining tests

The machining tests were conducted on a Mori Seiki NL 1500™ CNC lathe equipped with a special designed line assembled to fulfil the cryogenic cooling. The cryogenic fluid used in the tests was Liquid Nitrogen (LN_2), supplied to the cutting zone from a high-pressure storage dewar through a vacuum insulated pipe. Two copper nozzles with an internal diameter of 0.9 mm were used to direct the LN_2 simultaneously towards the tool flank and rake faces to improve its cooling capacity [9].

The adopted cutting tool was a semi-finishing insert VCEX110301LF1125 with a radius of 0.1 mm supplied by Sandvik Coromant™. The values of the cutting speed (V) and feed (f) adopted for the tests were 100 m/min and 0.1 mm/rev, respectively, chosen on the basis of a previous study made by Authors [6]. The depth of cut (d) was maintained constant as well and equal to 0.25 mm in order to achieve a semi-finishing cutting condition. The machining tests were performed under dry and cryogenic conditions. In order to avoid any tool wear effect on the experimental results, each specimen was turned with a new tool.

The experimental plan for the machining tests is reported in Table 1 and the sample machined geometry in Fig. 2.

Table 2. Experimental plan for the machining tests.

Machining strategy	f (mm/rev)	V (m/min)	d (mm)
Dry	0.1	100	0.25
Cryogenic	0.1	100	0.25

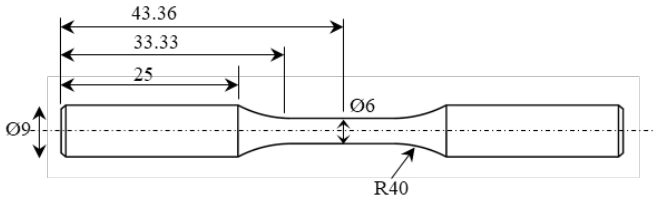

Fig. 2. Geometry of the CF specimen after machining.

2.3. Corrosion fatigue tests

The CF tests were carried out on the MTS™-322 hydraulic dynamometer adopting a force control mode. Tension–compression fatigue tests were conducted on the machined dog-bone samples under a sinusoidal wave form at a frequency of 10 Hz and a stress ratio (R) equal to -1.

The applied load was chosen to provoke failure at a reasonable number of cycles on the basis of the data reported in Table 1. The CF tests were conducted at three level of nominal stress amplitude (σ_a), namely 100 MPa, 110 MPa, and 120 MPa. The number of cycles (N_f) at complete failure of the specimen was recorded. During the tests, the samples were permanently immersed in the SBF solution, whose chemical composition is reported in [9]. To this purpose, a corrosion chamber made of poly(methyl methacrylate) was fixed to the sample's shoulder by means of an O-ring to prevent any leakage of solution.

Fig. 3 (a) shows the 3D model of the CF test arrangement while Fig. 3 (b) a photo of the experimental setup. Table 3 summarizes the experimental plan for the CF tests. Each test was repeated three times for each cooling condition to assure reproducibility of the results.

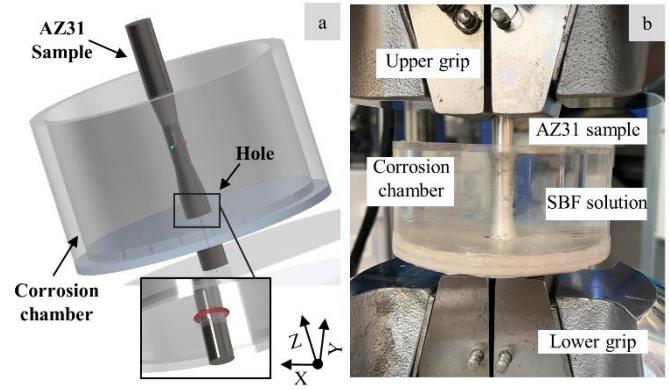

Fig. 3. Set-up of the CF tests: (a) 3D model (not to scale), (b) sample inside the SBF solution and mounted on the hydraulic dynamometer.

Table 3. Experimental plan for the CF tests.

Machining strategy	σ_a (MPa)	Force (N)
Dry/Cryogenic	100	2827
Dry/Cryogenic	110	3110
Dry/Cryogenic	120	3393

2.6 Characterization after corrosion fatigue testing

The Sensofar Plu-Neox™ optical profiler was used to scan the fracture surfaces after CF testing. Due to the high roughness of the fracture surfaces, the measurements were conducted via the focus variation mode employing a 20X confocal objective.

To evaluate the corrosion morphology, a FEI™ QUANTA 450 Scanning Electron Microscope (SEM) was used. The fracture surfaces of each sample were observed under Secondary Electron (SE) mode at different magnifications.

To correlate the corrosion extent after CF testing to the microstructural features, the microstructure of the broken samples was also examined. To this aim, they were cut along their longitudinal axis, then cold mounted, ground and polished. Acetic and picric acid aqueous solution was used as etch the grain boundaries. Finally, the microstructure observations were conducted using a Leica DMRE™ optical microscope equipped with a high-definition digital camera.

3. Results and discussion

3.1. Corrosion fatigue behaviour

The results of the CF tests are displayed and summarized in Fig. 4 and Table 4. The histogram shows the average number of fatigue cycles to failure at varying nominal stress amplitude. For this purpose, dry and cryogenic cooling histories are compared. The shown data emphasize that, regardless of the imposed stress, the samples processed with the LN_2 adduction endured a greater number of cycles than the corresponding dry cut samples, especially at the highest stress amplitude. The fatigue life of the cryogenic machined samples increased by 225%, 236%, and 265% at increasing mechanical load. These differences can be attributed to those surface integrity changes achieved when using cryogenic cooling, as described in §1 and already reported by the Authors [8, 9].

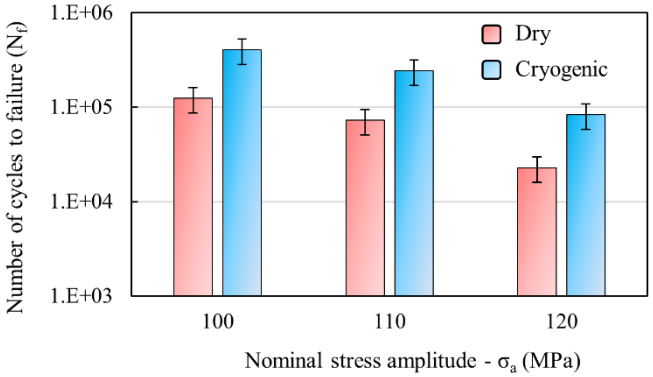

Fig. 4. Corrosion fatigue data for the dry and cryogenic machined samples at varying nominal stress amplitude.

Table 4. Number of cycles to failure for dry and cryogenic machined samples at varying imposed stress.

σ_a (MPa)	N_f (Dry)	N_f (Cryogenic)
100	124346	404193
110	72320	242896
120	22729	82937

Fig. 5. Example of broken dry (a), and cryogenic (b) machined samples after CF testing.

In particular, the presence of a thicker nanocrystalline layer in the case of the cryogenic machined samples generates greater resistance to plastic deformation, thus postponing the crack nucleation [6]. Along with grain refinement, also the presence of a compressive residual stress is useful to contrast the crack propagation [6].

The improved CF behavior at increasing mechanical load can be ascribed to the fact that the material is subjected to corrosion for a shorter time. Indeed, the lower the stress amplitude the higher the testing time, therefore the higher the surface material lost due to the corrosion phenomena.

Fig. 5 (a) and (b) show an example of dry and cryogenic machined samples broken after CF testing. It is worth noting that, in both the cases, the fatigue failure occurred at the gauge section, which witnesses the validity of the employed experimental procedure.

Figs. 6, 7 and 8 illustrate the samples fracture sites acquired through SEM observations together with the corresponding topographies for both the machining conditions at varying imposed stress. The three stages of fatigue failure, namely crack initiation (I), crack propagation (II), and final overload failure (III) can be pointed out by looking at both SEM images and topographies at the same time. Actually, the former give info about morphology whereas the latter provide details about heights. In general, the crack initiation sites are always located at the sample surface where corrosion pits tend to grow, as visible by irregular edges of the surface.

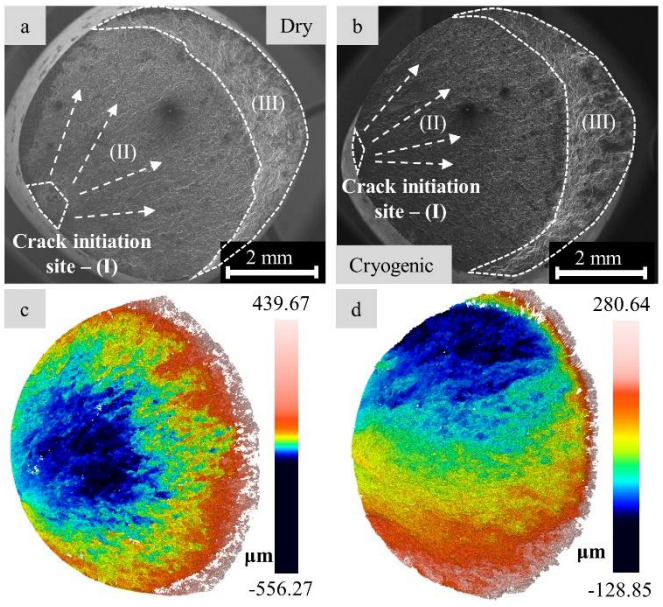

Fig. 6. SEM images (a, b) and corresponding surface topographies (c, d) of the fracture surfaces after CF testing at $\sigma_a = 100$ MPa.

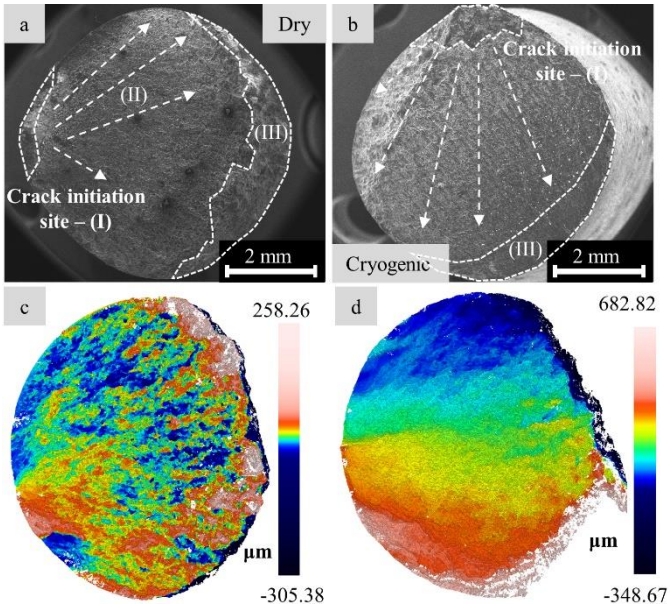

Fig. 7. SEM images (a, b) and corresponding surface topographies (c, d) of the fracture surfaces after CF testing at $\sigma_a = 110$ MPa .

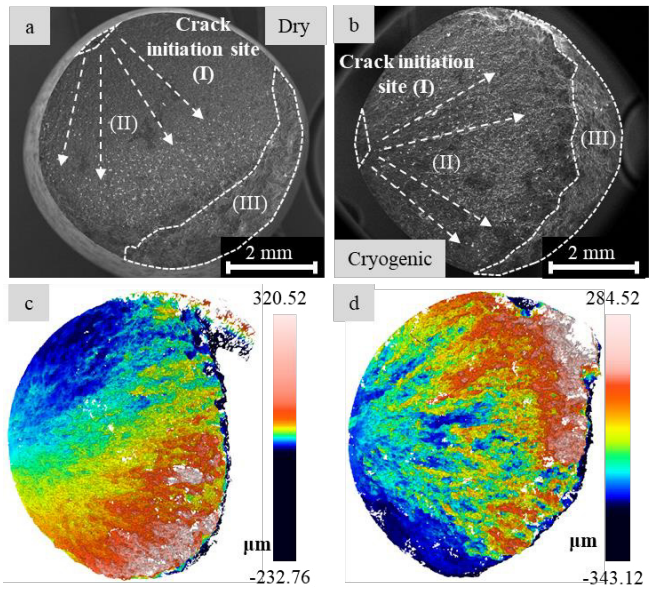

Fig. 8. SEM images (a, b) and corresponding surface topographies (c, d) of the fracture surfaces after CF testing at $\sigma_a = 120$ MPa .

Then, the fracture proceeds as indicated by the river marks departing from the crack initiation site (highlighted by white arrows in the figures). Finally, mechanical overloading takes over, leading to the sample catastrophic fracture. No macroscopic differences can be appreciated among the two machining conditions and applied mechanical load since both dry and cryogenic processed samples show similar surface fracture appearance.

4.2 Cross-sectional microstructures after CF testing

The cross-sectional microstructures below the samples surface are displayed in Fig. 9 as a function of the machining condition and imposed stress during CF testing.

Regardless of the applied load, the surfaces after CF tests appear corroded as witnessed by the presence of several corrosion pits along the edges. These pits are detrimental for fatigue resistance, since they act as nucleation sites for cracking, as visible on the dry sample tested at $\sigma_a = 110$ MPa that shows intergranular cracks (see Fig. 9 (c)).

Besides pitting, deformation twins are present within the grains adjacent to the fracture surface. Even some twins were already present in the as-delivered condition and then further increased during machining, the number of twins drastically multiplied as a consequence of CF testing. As a matter of fact, although the surfaces shown in Fig. 9 (a), (c) and (e), and those shown in Fig. 9 (b), (d) and (f) were generated by the same machining process, they significantly differ in terms of twins density. Specifically, it can be observed that the higher the distance from the fracture surface the lower the twinning intensity, and that a higher twinning intensity is visible at 110 MPa and 120 MPa compared to the sample tested at the lowest imposed stress.

The development of deformation twins can be explained on the basis of the cyclic loading during CF testing: the compressive load may result in twin formation, while a subsequent tensile load may cause detwinning as underlined in [11-12] in case of CF testing of magnesium alloys. Thus, the observed residual twins are the result of the competition between twinning in compression and detwinning in tension during the cyclic deformation. It is believed that the deformation twins can strongly contribute to both fatigue crack initiation and propagation because during cyclic loading the local strain concentration is relatively high at twin bands [13] as well as the twin boundaries are intrinsically brittle representing a favorable damage initiation site [14].

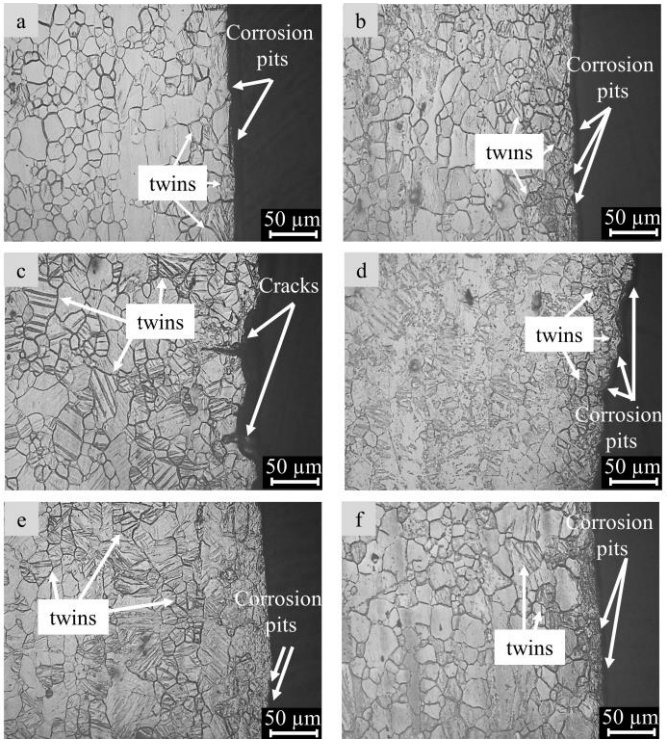

Fig. 9. Cross-sectional microstructure below the sample surface after CF testing: Dry $\sigma_a = 100$ MPa (a), Cryogenic $\sigma_a = 100$ MPa (b), Dry $\sigma_a = 110$ MPa (c), Cryogenic $\sigma_a = 110$ MPa (d), Dry $\sigma_a = 120$ MPa (e), and Cryogenic $\sigma_a = 120$ MPa (f).

By comparing dry and cryogenic samples, it can be noted that twinning appears less frequently in the latter case, especially at higher imposed stress. Zhu et al. [15] reported that larger grains tend more easily to deform by twinning than smaller grains.

Consistently, cryogenic machining, which results in smaller grains close to the machined surface (see the microstructures in Fig. 9), can lead to less deformation twinning during CF testing. In addition, in the case of finer grains, fatigue cracks encounter a higher fraction obstacle during their movement (grain boundaries), hence reducing the fatigue cracks tendency to grow, and, therefore, leading to higher fatigue life.

4. Conclusions

The present study evaluated the effect of machining cooling conditions on the corrosion fatigue behaviour of the AZ31 magnesium alloy.

To this purpose, samples were both dry and cryogenic machined and then subjected to corrosion fatigue tests at varying imposed stress.

The samples fracture surfaces were then analyzed using optical profiler, scanning electron microscope and the microstructures close to the machined surfaces by means of metallographic investigations.

The main findings can be summarized as follows:

- The cryogenic machined samples exhibited higher CF resistance than the corresponding dry ones, regardless of the imposed stress.
- The above-mentioned improved behaviour after cryogenic machining was attributed to the surface grain refinement induced by the work hardening favored by the very low temperatures and to the reduced number of deformation twins. The lower tendency of cryogenic machined samples to develop twinning during CF testing was again related to the reduced grain size.

Acknowledgements

This research was carried out in the framework of the project PRIN 201742RB8R_002 “Bionic” funded by the Italian Ministry of University and Research.

References

[1] Peron M., Torgersen J, Berto F. Mg and its alloys for biomedical applications: exploring corrosion and its interplay with mechanical failure. Metals 2017; 7(7): 252.

[2] Choudhary L, Raman RS, Hofstetter J, Uggowitzer PJ. In-vitro characterization of stress corrosion cracking of aluminium-free magnesium alloys for temporary bio-implant applications. Mat Sci Eng: C 2014;42:629-636.

[3] Hakimi O, Aghion E, Goldman J. Improved stress corrosion cracking resistance of a novel biodegradable EW62 magnesium alloy by rapid solidification, in simulated electrolytes. Mat Sci Eng C (2015);51:226-232.

[4] Gu XN, Zhou WR, Zheng YF, Cheng Y, Wei SC, Zhong SP, Chen LJ. Corrosion fatigue behaviors of two biomedical Mg alloys–AZ91D and WE43–in simulated body fluid. Acta biomater 2010;6(12):4605-4613.

[5] Antunes RA, De Oliveira MCL. Corrosion fatigue of biomedical metallic alloys: mechanisms and mitigation. Acta biomater 2012;8(3):937-962.

[6] Chen G, Fu Y, Cui Y, Gao J, Guo X, Gao H, Wu S, Lu J, Lin Q, Shi S. (2019). Effect of surface mechanical attrition treatment on corrosion

fatigue behavior of AZ31B magnesium alloy. Int J Fatigue 2019;127:461-469.
[7] Kasaeian-Naeini M, Sedighi M, Hashemi R. Severe plastic deformation (SPD) of biodegradable magnesium alloys and composites: A review of developments and prospects. J Magnesium Alloys 2021; article in press.
[8] Bruschi S, Bertolini R, Ghiotti A, Savio E, Guo W, Shivpuri R, Machining-induced surface transformations of magnesium alloys to enhance corrosion resistance in human-like environment. CIRP Annals 2018;67(1):579-582.
[9] Bertolini R., Bruschi S, Ghiotti A,.Pezzato L, Dabalà M. The effect of cooling strategies and machining feed rate on the corrosion behavior and wettability of AZ31 alloy for biomedical applications. Procedia Cirp 2017;65:7-12.
[10] Peron M, Bertolini R, Ghiotti A, Torgersen J, Bruschi S, Berto F. Enhancement of stress corrosion cracking of AZ31 magnesium alloy in simulated body fluid thanks to cryogenic machining. J Mech Behav Biomed Mater 2020;101:103429.
[11] Jafari S, Raman RS, Davies CH, Hofstetter J, Uggowitzer PJ, Löffler JF. Stress corrosion cracking and corrosion fatigue characterisation of MgZn1Ca0. 3 (ZX10) in a simulated physiological environment. J Mech Behav Biom Mater 2017;65: 634-643.
[12] Koike J, Fujiyama N, Ando D, Sutou Y. Roles of deformation twinning and dislocation slip in the fatigue failure mechanism of AZ31 Mg alloys. Scripta Mater 2010;63(7):747-750.
[13] Bernard JD, Jordon JB, Horstemeyer MF, El Kadiri H, Baird J, Lamb D, Luo AA. Structure–property relations of cyclic damage in a wrought magnesium alloy. Scripta Mater 2010;63(7):751-756.
[14] Wu Z, Curtin WA. Brittle and ductile crack-tip behavior in magnesium. Acta Mater 2015;88:1-12.
[15] Zhu YT, Liao XZ, Wu XL, Narayan J. Grain size effect on deformation twinning and detwinning. J Mater Sci 2013; 48(13): 4467-75.